Optimizing green hydrogen production from wind and solar for hard-to-abate industrial sectors across multiple sites in Europe

Optimizing green hydrogen production from wind and solar for hard-to-abate industrial sectors across multiple sites in Europe

Authors: Marcel Stolte[a,b], Francesco Demetrio Minuto[a,b], Andrea Lanzini[a,b]*

* *Corresponding author: andrea.lanzini@polito.it*

a Department of Energy, Politecnico di Torino, Corso Duca degli Abruzzi 24, 10129 Torino, Italy

b Energy Center Lab, Politecnico di Torino, Via Paolo Borsellino 38/16, 10138 Torino, Italy

Abstract

This article analyzes a power-to-hydrogen system, designed to provide high-temperature heat to hard-to-abate industries. We leverage on a geospatial analysis for wind and solar availability and different industrial demand profiles with the aim to identify the ideal sizing of plant components and the resulting Levelized Cost of Hydrogen (LCOH). We assess the carbon intensity of the produced hydrogen, especially when grid electricity is utilized.

A methodology is developed to size and optimize the PV and wind energy capacity, the electrolyzer unit, and hybrid storage, by combining compressed hydrogen storage with lithium-ion batteries. The hydrogen demand profile is generated synthetically, thus allowing different industrial consumption profiles to be investigated.

The LCOH in a baseline scenario ranges from 3.5 to 8.9 €/kg, with the lowest values in wind-rich climates. Solar PV only plays a role in locations with high PV full-load hours. It was found that optimal hydrogen storage can cover the users' demand for 2-3 days.

Most of the considered scenarios comply with the emission intensity thresholds set by the EU. A sensitivity analysis reveals that a lower variability of the demand profile is associated with cost savings. An ideally constant demand profile results in a cost reduction of approximately 11 %.

Keywords: Power to Hydrogen, Optimization, Energy storage, Renewable energy, Electrolysis, Green hydrogen

1. Introduction

1.1 The use of hydrogen in industry

Industry is one of the largest emitters of greenhouse gases and contributes by 25 % to the global yearly CO_2 emissions of the energy system [1]. Although electrification has the potential to decarbonize many applications in other sectors, not all industrial processes can be powered by electricity. Hard-to-abate sectors, which consist of industries that face significant challenges in reducing their greenhouse gas emissions due to the nature of their processes and energy requirements, are particularly affected. These industries are often characterized by a large high-temperature heat demand, which poses significant challenges and electricity-based heating options are not a feasible solution for many users. Green hydrogen can be an interesting option to provide high-temperature process heat and replace traditional natural gas-based supply [2].

However, decarbonizing industrial heat presents a multifaceted challenge, with solutions that vary according to the specific process. There is no one-size-fits-all solution to this complex issue. The current options for electrification encounter difficulties when it is necessary to deal with high-temperature heat of more than 500°C, which makes hydrogen a more favorable option in these cases. This is particularly relevant for the Iron and Steel, Concrete & Cement and chemical industries. High-temperature process heat is crucial in the cement industry, particularly for rotary kilns (1400-1500°C) and pre-calciners (600-700°C). Although some redesigning may be necessary to accommodate the different properties of hydrogen in rotary kilns, their environment is generally favorable[2], [3]. The ceramics industry, in a similar way to the cement industry, can be a relevant sector for the use of green hydrogen. The drying processes in this industry are energy intensive and are followed by firing to temperatures of between 800 and 2000ºC [4]. Hydrogen is already used as a catalyst in the oil-refining industry. However, the refineries in this sector present fewer opportunities for hydrogen use as a thermal energy carrier. This is because waste products generated during refining are utilized for heat generation, and input fuels are therefore readily available at a low cost [2]. For the pulp and paper industry a large electrification potential exists. Only a minor share of the heat demand consists of temperatures > 200°C, and byproducts that can then be used thermically are generated. As a result, hydrogen uptake has to deal with a less favorable environment [5].

However, fully substituting natural gas with hydrogen in process heat applications may not be technically feasible, without significant equipment modifications, as the difference in chemical properties introduces additional complexity. Hydrogen has a higher flame speed and burns at a higher temperature than natural gas, which can lead to increased NOx emissions and require modifications to existing combustion systems to prevent material stress and damage [6]. Therefore, a fuel transition period with increasing hydrogen blending could be a convenient solution [7].

A realistic industrial demand profile is crucial for an accurate analysis of the power-to-hydrogen (PtH) production in industry. Moreover, machine-learning techniques already exist, in the context of electricity demand, to generate and reconstruct hourly load profiles [8]. Conversely, open access data on heat demand profiles or complete methodologies to generate them with an hourly

resolution are scarce, especially for large industries. Thus, synthetical load profiles are needed to overcome these issues and generalize the analysis for different industries that have a demand for high temperature process heat.

Profiles of industrial sites with a demand for high-temperature process heat are generally characterized by a high baseload and demonstrate a low dependency on external parameters, such as the weather conditions. Nevertheless, significant demand fluctuations may occur, depending on the considered industrial processes. Jesper et al. [9] analyzed 797 natural gas industrial consumption profiles in Germany and divided the profiles into clusters using k-means clustering. They used these clusters as a basis to generate synthetic load profiles with a daily resolution.

1.2 Green hydrogen production

Various pathways can be followed to produce low emission hydrogen. Apart from water electrolysis from renewables, steam methane reforming (SMR) with carbon capture and biomass gasification can also be used as alternative methods. Nevertheless, its production by means of water electrolysis is the most promising of all the green hydrogen production routes and will likely play a central role in the future production of hydrogen [10].

However, several challenges will have to be tackled and certain requirements will need to be satisfied before it can be deployed on a large scale. Given the highly energy-intensive nature of hydrogen production, achieving the desired reductions in greenhouse gas emissions depends on being able to ensure that the used electricity is sourced from renewable generation. Failure to do so may lead to increased emissions, compared to those from conventional natural gas or the use of gray hydrogen [11]. Moreover, the additional impact of the dedicated renewable infrastructure should be considered [12]. Another significant obstacle to the deployment of green hydrogen within the industry is the substantial capital cost of the required equipment, which hinders its economic feasibility for decarbonization [2], [13]. For this reason, the European Union has established certain requirements and incentives for green hydrogen. Such incentives for green hydrogen should be in line with the regulatory principles of temporal and geographic correlation and of additionality[14], [15]. Support schemes for green hydrogen already exist at both the European and the national/regional levels. Examples include the hydrogen bank, which provides incentives per kg of hydrogen produced in the form of an auction, or CAPEX incentives for hydrogen use in hard-to-abate industries [15].

Green hydrogen production and its storage for decarbonization purposes have been extensively studied in the scientific literature from various perspectives. In microgrids, hydrogen serves as an energy vector, with benefits seen in combination with batteries [16]. Hybrid energy storage concepts, including batteries and hydrogen, have also been investigated for power-to-hydrogen systems. Compressed hydrogen storage has been considered for in the present study because it is already available commercially. However, other innovative technologies, such as adsorption-based storage, are also being developed [17]. The results are less unequivocal for battery storage. In a case study on an islanded community, Novo et al. optimized the local energy system and also investigated the optimal battery storage size [18]. Martinez Lopez et al. [19] reviewed the dynamic operation of electrolyzers for green hydrogen production, and found that battery storage tends to

increase the overall costs, particularly for grid-connected systems. Ibanez Rioja et al. [20] analyzed the optimization of an off-grid hydrogen production plant supplied exclusively by solar PV and wind turbines, and which included Li-ion battery storage. The results revealed that wind is the most economical energy source and PV and Battery storage could only become part of the optimal solutions in future scenarios after 2035. The considered location was in Finland, which has comparably low solar radiation. Dufo-López et al. [21] optimized the sizes of PV, wind turbines, and electrolyzer, as well as the control strategy for a hydrogen production system. In this case, the LCOH varied over a broad range of between 4.7 €/kg and 16.1 €/kg, depending on configuration and location of the system. They focused on the operation strategy and precise modelling of the components but did not cover the demand or storage aspects.

In a techno-economic analysis conducted by [22], the authors explored a price-based control system implemented in a 1.5 GW offshore PtH system. They utilized real wind turbine data obtained from a 2.3 MW floating offshore turbine. The control strategy was able to reduce the LCOH by 10 to 46 %, with the lowest value being 6.04 €/kg. It is worth noting that this value did not factor in the optimization of the plant sizes. Hofrichter et al. [23] investigated the optimal ratio between PV or Wind capacity and electrolysis capacity for locations with different full-load hours. The LCOH from wind farms was lower than that from PV-electricity. In the solar PV case, the optimal Electrolyzer/RES ratio was determined as 3-5. The electrolyzer was modelled using a detailed efficiency function (Energiepark Mainz). The renewable energy plant sizes were selected manually, without using optimization algorithms. The main limitation of the study, as mentioned in the text, was its assumption of a fixed cost for renewable electricity generation of 0.04 €/kWh, independently of the full-load hours.

Other studies have focused specifically on simulating power-to-hydrogen systems in the hard-to-abate industry sector. Elsheikh et al. [24] conducted a detailed investigation on the use of hydrogen in the steel industry using the DRI-EAF route and compared it, regarding emissions and costs, with alternative steelmaking pathways. The paper included the analysis of solar PV and upstream grid-based hydrogen production. In a later work, the authors expanded the analysis to include wind energy and conducted the analysis on different locations with different renewable characteristics. They observed benefits when combining solar and wind resources to reduce renewable volatility [25].

Marocco et al. [26] assessed the substitution of natural gas with hydrogen for high-temperature heat in a case study of a steel plant in northern Italy. They used an MILP approach to optimize the sizes of the compressor, electrolyzer, hydrogen storage, and the operational strategy. However, the study did not assess the renewable energy production itself and considered a fixed-price grid supply. In a subsequent work [27], the authors tackled these gaps and added electricity generation from solar PV and battery storage to the analysis and assessed different sensitivities regarding the electricity purchase price. The obtained LCOH was in the 3.5 to 7 €/kg range. Superchi et al. [11] explored green hydrogen production on a windfarm located in Greece used to supply a steel plant. The study included hydrogen and battery storage, and they identified hydrogen storage as being crucial to increase the green hydrogen share. The optimal configuration considered in the article reached an LCOH of 5.7 €/kg. Mingolla addresses the effect of emission caps for green hydrogen

production, doing an extensive analysis across European ammonia plant locations. Their findings highlight the benefits of moderate emission caps, which reduce emissions and still achieve low LCOH [28].

1.3 The identified research gaps and the contributions of this article

Although the previously mentioned studies have offered valuable insights into hydrogen production or its industrial applications, a significant portion of the literature has tended to concentrate on either the hydrogen consumption side or has simulated general hydrogen production applications, without taking into account specific industrial demand profiles. Consequently, these articles did not consider any temporal mismatch problems between hydrogen production and its demand. However, when examining the role of energy storage in a study, this aspect should not be overlooked. Moreover, a gap in generalization exists regarding the impact of fluctuations on the demand profile, which plays a crucial role in influencing the optimal plant layout and the achieved LCOH. Therefore, it is essential to consider these variations when evaluating the efficacy of energy storage solutions to meet hydrogen demand requirements across different operational scenarios. The existing studies have often relied on case studies without systematically exploring the available renewable resources and lack a generalization approach. Furthermore, there is limited research on optimizing PtH in the context of hard-to-abate industries, particularly those that have assessed both wind and solar in combination with batteries and hydrogen storage. Table 1 provides an overview of the literature on PtH and compares the contributions regarding the main aspects of this study.

Table 1: Literature overview of similar articles regarding specific features

	This Study	**Dufo-López**[21]	**Hofrichter** [23]	**Ibanez-Rioja**[20]	**Marocco** [27]	**Elsheikh** [25]	**Superchi** [11]	**Mingolla** [28]
Geospatial analysis	Yes		Yes			Yes		Yes
Load profile sensitivity	Yes							
Grid price sensitivity	Yes	Partial			Yes	Partial	Yes	Partial
PV	Yes	Yes	Yes	Yes	Yes	Yes		Yes
Wind	Yes	Yes	Yes	Yes		Yes	Yes	Yes
Li-Ion battery	Yes			Yes	Yes	Yes	Yes	Yes
Hydrogen storage	Yes	Yes			Yes	Yes	Yes	Yes
Emission assessment	Yes				Yes	Yes	Yes	Yes

Thus, in order to close these research gaps, the article provides the following contributions:

- It evaluates the optimal design and operation of a Power-to-Hydrogen system across various contexts of available renewable energy, thereby facilitating its generalization for different locations. The analysis considers what renewable inputs are the most suitable for this purpose and examines the impact of combining PV and wind power as electricity sources.
- It employs a comprehensive methodology to analyze the effects of the variability of the demand profile, thereby enabling the results to be generalized to different user profiles.
- It investigates the economic viability of different energy storage options in the context of a hard-to-abate industrial site and considers the sensitivities regarding the electricity price.

2. Methodology

Figure 1 displays the Power-to-Hydrogen system that has been investigated in this study. The renewable electricity production of the PV plant and wind turbines provides input for the electrolyzer. A Li-ion battery, charged exclusively by renewables, provides load shifting abilities. The compressed hydrogen storage, located downstream of the electrolyzer, allows the produced hydrogen to be stored. This additional storage capacity increases the flexibility of the system. The electrical grid connection enables the demand to be covered in periods of low renewable

availability and surplus renewable production to be acquired when the capacity limits of hydrogen storage and the electrolyzer are surpassed.

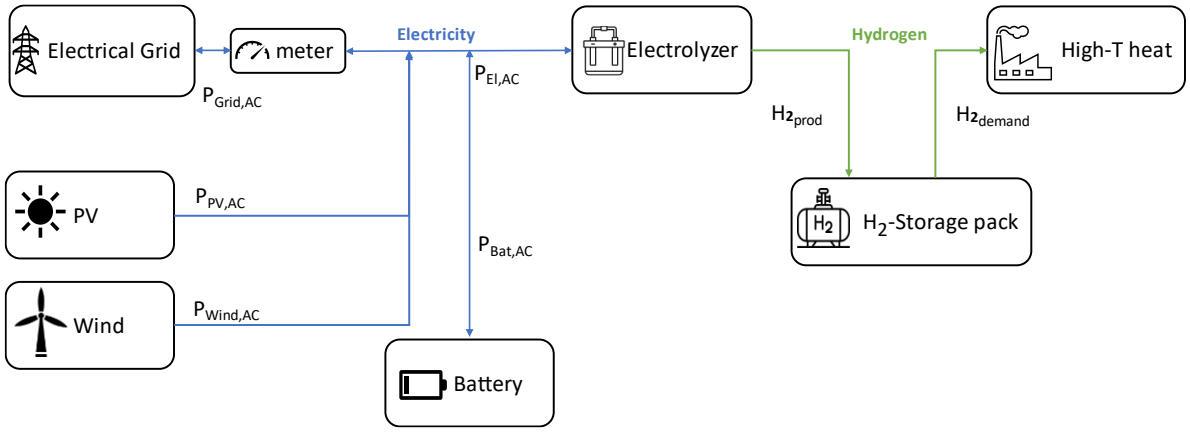

Figure 1: Model scheme of the system

2.1 Optimization Framework

An energy system model, which characterizes the system shown in Figure 1, has been developed using Python. The sizing of the system has been optimized using Particle Swarm Optimization (PSO) and employing the "pyswarms" library [29]. It is essential to accurately configure the hyperparameters, which requires a delicate balance between convergence and exploitation, and was achieved through a grid search [30]. A rule-based strategy within the objective function of the algorithm manages and balances the operation of the system on an hourly basis.

The control strategy is written in such a way to achieve the following objectives:

- of satisfying the users' hydrogen demand on an hourly basis
- of maximizing the utilization of renewable electricity
- of minimizing the withdrawal of electricity from the electric grid.

In order to accomplish these objectives, the strategy has been guided by the following principles:

- employing grid electricity exclusively when the hydrogen demand could not be satisfied by renewable sources.
- prioritizing the charging of hydrogen storage over the battery system.

The management of two distinct energy storage systems introduces significant complexity, which is further compounded by the grid connection of the overall system. Therefore, a systematic approach was considered imperative to oversee the operation of the system and to ensure adherence to the operational principles, while maintaining manageability. Different operational conditions were delineated to facilitate the management of the complex system in a maintainable manner and to simultaneously be aligned with the control objectives. Five inequalities, which can be found in Appendix A, were assessed for each hour. The results of the inequality constraints were then combined to form operational cases. As a result of redundancy and logical exclusion, 10 distinct operational cases emerged (see Table A.1). Each of these cases was associated with a specific code

that was aligned with the operational objectives that govern the system. An overview of the optimization framework can be found in Appendix A Figure A.2.

2.1.1 Site selection across Europe

A methodological analysis of solar PV and wind energy potential across Europe was considered crucial to select representative sites for the study. The data used to assess the renewable energy potential across Europe was sourced from two primary datasets: the Global Solar Atlas and the Global Wind Atlas. The Global Solar Atlas provides the specific photovoltaic power output kWh/kWp and offers direct insight into full-load hours. This metric was chosen over Global Horizontal Irradiance to mitigate distortions caused by such factors as temperature variations and radiation composition. The dataset relies on different meteorological datasets, including ERA5 [31]. Similarly, the Global Wind Atlas offers detailed wind climate information, which, in this study, was used to determine the mean wind speed at a height of 100 m, coherently with the later profile selection. This dataset was derived from ERA5 data, which was refined and downscaled considering the topography of the locations [32].

These datasets were chosen because of their comprehensive coverage and reliability in providing key indicators for renewable energy assessments. A grid that covered all of Europe was generated to facilitate the spatial analysis. Each grid cell corresponds to a 1-degree latitude/longitude base, thereby ensuring uniform coverage across the region of interest. The zonal mean of each grid zone was computed for both the wind speed and full-load PV hours.

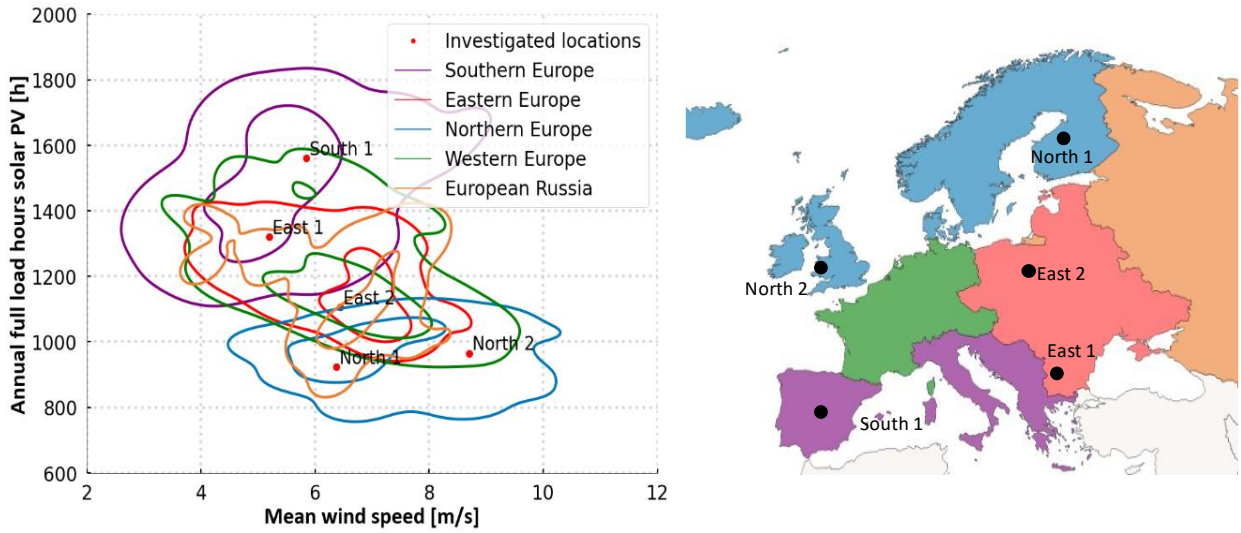

Figure 2: The authors' own elaboration of the mean windspeed and annual full-load hours of the solar PV distribution across Europe based on [31], [32], including a visualization of the selected locations

Figure 2 illustrates the distribution of the solar and wind energy potential across the European macro-regions defined by the UN M49 standard [33], and further separates the large eastern European area into eastern Europe and European Russia. The areas enclosed by the lines represent the distribution of renewable energy resources in the respective regions. The density of measurements increases toward the inner lines. This means that the center of the areas indicates

the most frequent renewable availability for that region. Most of the points in southern Europe show a high solar PV potential, whereas this trend shifts toward wind resources in northern Europe.

A strategic selection of representative sites, which are denoted by red points in Figure 2, was conducted on the basis of this density distribution. This was done by selecting the location closest to the most frequent renewable availability. The selection was limited to 5 points, as an analysis of each grid cell would have exceeded the available computational resources. Nevertheless, due to their representative characteristic these five sites cover a broad range of geographic and climatic conditions and ensure a robust assessment methodology.

Table 2: Selected European locations

Denomination	**South 1**	**East 1**	**East 2**	**North 1**	**North 2**
Country	Spain	Bulgaria	Poland	Finland	The United Kingdom
NUTS 2	Estremadura	Yugozapaden Planning Region	Masovian Regional	North & East Finland	North-West England
Latitude	40.1	43.0	53.3	64.12	53.9
Longitude	-5.6	23.4	21.2	24.5	-3.0
Mean windspeed [m/s] [34]	5.85	5.19	6.44	6.37	8.70
PV full-load hours [h]	1,563	1,320	1,106	924	965

2.1.2 Electricity sources

The renewable electricity inputs were modelled considering a dedicated wind farm and a solar PV plant. PV electricity generation profiles, with an hourly resolution, were obtained from the EU Photovoltaic Geographical Information System (PVGIS) for the five locations. Moreover, the tilt and azimuth angles of the fixed-mounted racks were also optimized by means of PVGIS, choosing crystalline silicon module technology. Factors such as power losses in the inverters and cables, dirt on the modules, and degradation were considered, and an overall system loss value of 14% was obtained. For further details, the reader can refer to the PVGIS methodology [35]. The wind farm was simulated using Renewables Ninja, a platform built upon NASA's Merra2 dataset, which has undergone reanalysis and bias correction [36]. Vestas V136 4.0, set at a hub height of 100 m, was the turbine model that was employed, and hourly electricity generation values were obtained. Hourly solar radiation and wind speed data, along with the corresponding hourly capacity factors and wind turbine power curve, can be found in Appendix B. supplementary data.

The electrolyzer was interconnected with the electric grid, thereby providing the capability of bridging periods of low renewable energy production. This setup enables the users' demand to be fulfilled, even during such periods, thus mitigating the need for excessive renewable generation capacities. The electricity price for the industrial site was assumed to remain constant in the baseline scenario throughout the year at a rate of 150 €/MWh, on the basis of Eurostat data for non-domestic users that have an annual consumption of 70-150 GWh [37]. As part of a sensitivity

analysis, the electricity price was varied between 50 and 250 €/MWh, thereby representing extreme cases. Grid remuneration for surplus electricity feed-in was evaluated at 70 % of the acquisition price. This ratio was determined on the basis of historical data from 2018 to 2022, derived from the ratio of electricity wholesale prices-to-electricity prices for industrial consumers. Data from Eurostat and Bundesnetzagentur [37], [38] were used for this analysis. The electricity sale value was later included in the LCOH calculation.

The use of grid electricity comes at the cost of reduced greenhouse gas savings. To be classified as renewable under EU regulations, hydrogen has to achieve a greenhouse gas emission intensity of less than 3 kg_{CO2}/kg_{H2} [39]. In this study, we calculated the emission intensity by multiplying the amount of used grid electricity by the average European grid emission factor of 250 gCO2/kWh for the year 2022 [40]. This choice is further discussed in Chapter 4.

Although it is crucial to achieve the emission threshold, other legislative aspects defined in the EU's Renewable Fuels of Non-Biological Origin (RFNBO) framework should be considered on a project-by-project basis [15]. These additional criteria, including temporary, additionality, and geographic requirements, are essential to classify hydrogen as renewable. We can reasonably assume that the production facilities for electricity generated from on-site renewable sources are located within the same bidding zone as the electrolyzer and constructed no earlier than 36 months before hydrogen production begins. However, the requirements regarding the electricity withdrawn from the grid are more challenging. Given the variability across the different bidding zones, markets, or eventual power purchase agreements, it is not possible to uniformly assess and generalize compliance with these requirements. Therefore, this study focuses solely on hydrogen emission intensity.

2.1.3 Electrolyzer

A PEM electrolyzer was selected for simulation, due to its favorable characteristics during load fluctuations in conjunction with volatile renewable energy production. Because of the considered one-hour resolution of the demand profile and the capabilities of the PEM electrolyzer to adapt to load fluctuations, such dynamic effects like startup have been neglected in this study.

The efficiency of an electrolyzer is influenced by various factors. These factors include activation losses, ohmic resistance, and mass transport within the cell, all of which depend on the electrolyzer load factor P_{el}. To account for these influences, Rezaei et al. [41] used an electrolyzer efficiency function that depends on P_{el}, which was based on experimental data by Kopp [42]. This function is characterized by a peak efficiency in part-load and also considers future technology improvements. The calculation of the efficiency η is described by the following equations:

For $P_{el} < 15\ \%$

$$\eta = \left(0.0005 \cdot P_{el}^5 - 0.0061 \cdot P_{el}^4 + 0.2372 \cdot P_{el}^3 - 4.2014 \cdot P_{el}^2 + 36.675 \cdot P_{el} - 62.87\right) \cdot 1.0025^{2024-2020} \quad (1)$$

For $P_{el} \geq 15\ \%$

$$\eta = \ (-0.149 * \mathrm{P}_{el} + 74.977) \cdot 1.0025^{2024-2020} \quad (2)$$

Equations (1) and (2) not only compute the electrolyzer efficiency for a given load factor but also allow the determination of the electricity consumption. This aspect is crucial when the hydrogen demand from end-users is known, and the corresponding electrical load has to be calculated. To achieve this, efficiency mappings are generated at 0.1% intervals across all load factors and utilized as a lookup table. This simplifies the calculation of the electrolyzer's electricity demand, reduces complexity in the control strategy, and minimizes computational expenses.

2.1.4 Hydrogen Tank

The Hydrogen Tank plays a crucial role in absorbing any excess production from renewables, and thereby increases the share of self-produced hydrogen. Its placement downstream of the electrolyzer represents a fundamental advantage of this storage technology for PtH systems, and it enhances supply security, particularly in the case of electrolyzer faults. The electrolyzer output pressure was set at 30 bar, which allowed the simplification of no further hydrogen compression to be introduced, as the input pressure of the hydrogen required by the burner was significantly lower than the electrolyzer output pressure [43]. The state of charge of the storage tank was updated at each time step on the basis of the hydrogen production and demand, thereby ensuring a precise utilization and management of the stored hydrogen.

2.1.5 Battery storage

The role of the battery is to add flexibility to the electrical side of the model and therefore to increase the self-consumption of renewable energy and the operating hours of the electrolyzer. This also reduces the need for grid withdrawal. Li-ion, which was selected because of its advantageous characteristics, such as high efficiency, compact storage densities, and robust cyclic capabilities, emerged as a suitable choice among the available storage technologies. This is also why Li-ion has been the preferred technology in recent utility scale installations and has been considered for the vast majority of new installations [44]. Operating with a specified roundtrip efficiency of 85%, the battery utilization is strategically controlled within a defined state of charge (SOC) window that ranges from 15 % to 95 %, to preserve the lifetime of the battery [45]. The energy management system computes the charging/discharging power for every hour on the basis of the system requirements. The model then updates the state of charge for each time step, taking into account the charging/discharging efficiencies, thereby ensuring accurate tracking of the energy flows and enabling the storage system to be effectively managed throughout the simulation period.

2.2 Synthetic load profile generation

We used a methodology proposed by Jesper [9] for the generation of the thermal demand profiles of industrial users who have a process heat demand. Cluster 0, hereafter nominated heavy industry cluster, was selected to characterize high-temperature applications in heavy industry for both weekdays and weekends, due to its minimal sensitivity to ambient temperature fluctuations. The profiles are generally characterized by a lower consumption during the weekends and holidays. A

normal distribution of consumption was applied for weekdays and weekends to introduce temperature independent variability into the daily profiles, utilizing the standard deviations of the heavy industry cluster. We adopted the daily consumption distribution method proposed by Lauterbach [46] to transition from a daily to an hourly resolution. This approach assigns a specific share of the daily consumption to each hour of the day, thereby facilitating the refinement of the profiles from a daily to an hourly resolution. The final load profile is depicted in Figure 3. The coefficient of variation (CV), defined as the ratio of the standard deviation to the mean, is 0.41 for this profile.

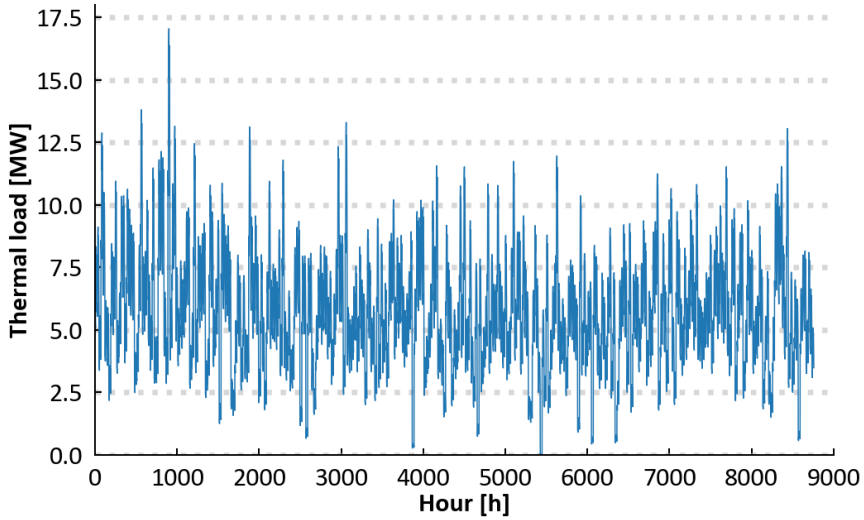

Figure 3: Thermal demand of the industrial site to be substituted with hydrogen

We needed to scale the normalized profile to the overall yearly hydrogen demand to ensure the obtained profile accurately reflected the thermal demand. An analysis of the Best Available Techniques reports [47], indicated that, on the basis of the average energy consumptions per ton of product and typical production quantities, the overall yearly thermal demand in many cases fell within the 25-100 GWh/year range [47]. On the basis of this data analysis, we scaled the normalized load profile to align with a total yearly consumption of 50 GWh. It is worth noting that these values are not representative of the steel industry, which often exhibits significantly higher consumption values.

The daily variability was further explored, in a sensitivity analysis, to broaden the scope of the analysis to other profiles present in the literature by adjusting the standard deviations of the heavy industry cluster. However, the other settings of the synthetic thermal load profile were maintained. Thus, 5 profiles with different coefficients of variation and a completely flat profile were obtained. The effects of the different demand profiles on the plant optimization are investigated in Chapter 3.3.

From the thermal load profile, the corresponding hydrogen demand $P_{H2,dem,t}$ must be calculated every timestep t. This is done considering the lower heating value of hydrogen LHV_{H2} of 33.33 kWh/kg.

$$P_{H2,dem,t} = \frac{P_{thermal,t}}{LHV_{H2}} \quad (3)$$

2.3 Evaluation metrics

The evaluation metrics spread across economic values and are useful to describe the system as well as environmental impacts. An effective size optimization relies on a well-defined objective function, which should include the definition of the cost functions. This function is then evaluated using relevant metrics that encompass both economic and environmental considerations. The metrics should include considerations on the component sizes and environmental indicators. In order to be able to calculate the LCOH, the costs have to be evaluated.

$$crf_j = \frac{(1+i)^{n_j} \cdot i}{(1+i)^{n_j} - 1} \quad (4)$$

The capital recovery factor, crf, is calculated for each system component j, considering the component lifetime n_j and the discount factor i. By factoring in the specific lifetimes of the components, we ensure that more frequent replacements of battery storage and electrolyzer are reflected in the LCOH.

$$EAC = \sum_{j=1}^{M} crf_j \cdot Inv_j + O\&M_j \quad (5)$$

We obtain the equivalent annual cost EAC of each component j by multiplying the capital recovery factor, crf, with the investment costs of the components, Inv. Also, the Operation and Maintenance cost, $O\&M$ are added.

The levelized cost also includes the cost of electricity taken from the grid, C_{grid}, and the hydrogen production, $P_{H2,t}$. The annualization of investment costs allows for the simulation of the system and calculation of the LCOH based on a 1-year simulation timeframe. This method avoids the computational burden associated with multi-annual simulations, while still providing accurate cost assessments.

$$LCOH = \frac{EAC + C_{grid} - R_{grid}}{\sum_{t=1}^{8760} P_{H2,t}} \quad (6)$$

In order to consider a realistic plant size, the revenues from the selling of electricity R_{grid}, are only considered after the optimization of the plant sizes. They are not included in the objective function as this would distort the result to a great extent and could incentivize the system to sell electricity to the grid and increase the installed renewable capacity.

$$OBJ = \frac{EAC + C_{grid}}{\sum_{t=1}^{8760} P_{H2,t}} \quad (7)$$

Apart from the cost metrics, the environmental impacts are also assessed using the share of electricity that comes from the dedicated renewable energy plants used for electrolysis. This share of hydrogen, which is derived from self-produced renewable energy, φ_{RES}, can be calculated as

$$\varphi_{RES} = \frac{\sum_{t=1}^{8760}(P_{RES,AC,t} - P_{grid,inj,t} - P_{bat,loss,AC,t})}{\sum_{t=1}^{8760}(P_{RES,AC,t} + P_{grid,wdl,t} - P_{grid,inj,t} - P_{bat,loss,AC,t})} \quad (8)$$

where $P_{RES,AC}$ is the AC power output of the renewables, $P_{grid,inj,AC}$ and $P_{grid,wdl,AC}$ are the power injection into and withdrawal from the grid, and $P_{bat,loss,AC}$ are the losses due to the charging and discharging processes of the battery.

Moreover, the emission factor, ef_{H2}, in kg_{CO2}/kg_{H2} of the produced hydrogen, is calculated as:

$$ef_{H2} = \frac{ef_{grid} \cdot \sum_{t=1}^{8760} P_{grid,wdl,t}}{\sum_{t=1}^{8760} P_{H2,t}} \quad (9)$$

This evaluation takes into account the emissions of the electricity acquisition by using the grid emission factor, ef_{grid}, the grid withdrawal, $P_{grid,wdl}$, and the quantity of the produced hydrogen, P_{H2}, in kg.

The φ_{El} ratio expresses the installed renewable power generation capacity in relation to the nominal power of the electrolyzer.

$$\varphi_{EL} = \frac{P_{wind,nom} + P_{PV,nom}}{P_{EL,nom}} \quad (10)$$

The storage duration, φ_{H2st}, is calculated in hours considering the capacity of the hydrogen storage in kWh. This capacity is divided by the hourly average hydrogen demand in kg and the Lower heating value of hydrogen LHV_{H2} in kW.

$$\varphi_{H2st} = \frac{E_{H2st}}{P_{H2,dem,av} \cdot LHV_{H2}} \quad (11)$$

The levelized cost of electricity (LCOE) is used to obtain insights into the electricity generation cost of the renewables at the different locations. It is calculated considering the discounted cashflows, that is, those consisting of CAPEX and the operation and maintenance costs as well as the discounted electricity production, El_{Gen}, over the lifetime, N, of the renewables.

$$LCOE = \frac{\sum_{t=0}^{N} \frac{(CAPEX_t + O\&M_t)}{(1+i)^t}}{\sum_{t=0}^{N} \frac{El_{Gen}}{(1+i)^t}} \quad (12)$$

The metrics are based on input assumptions and are summarized in Table 3. For further details, the reader can refer to Chapter 2.1 and Table A.2 in Appendix A.

Table 3: Model input assumptions for the base case

Parameter	Assumption	Reference
PV plant		
CAPEX	1,048 €/kWp	[45]
OPEX	20 €/kW	[45]
Lifetime	25 years	[45]
Orientation	Fixed mounted with optimized orientation angles	
Losses	14 %	[35]
Wind turbine		
CAPEX	1,261 €/kW	[45]
OPEX	43 €/kW/year	[45]
Lifetime	30 years	[45]
Turbine model	Vestas V136 4MW	[34]
Hub height	100 m	[34]
Electrolzyer		
CAPEX	1,099 €/kW	[48]
OPEX	48 €/kW/year	[48]
Efficiency	Efficiency curve based on load factor	[42]
Lifetime	50,000 h	[49]
Battery storage		
CAPEX	€/kW = 230*storage duration +249	[45]
OPEX	2.5 % of CAPEX/year	[45]
RTE	85%	[45]
Lifetime	10 years	[45]
SOC limits	0.15-0.95	[45]
Hydrogen storage		
CAPEX	700 €/kg	[50]
OPEX	2 % of CAPEX /year	[48]
Lifetime	20 years	[48]
Other inputs		
Electricity cost	150 €/MWh	[37]
Electricity selling price	70 % of electricity cost	[37], [51]
Grid electricity emission factor Europe	250 gCO2/kWh	[40]
Discount factor	5 %/year	[24]

3. Results and Discussion

The results regarding the economic analysis and optimal sizes for green hydrogen production for different European sites are presented in Chapter 3.1, while Chapter 3.2 presents the results of a sensitivity analysis on electricity costs, and also investigates the plant size metrics. Furthermore, the results of a sensitivity analysis that utilized different input profiles to explore the impact of demand fluctuations are presented in Chapter 3.3.

3.1 Levelized Cost of Hydrogen

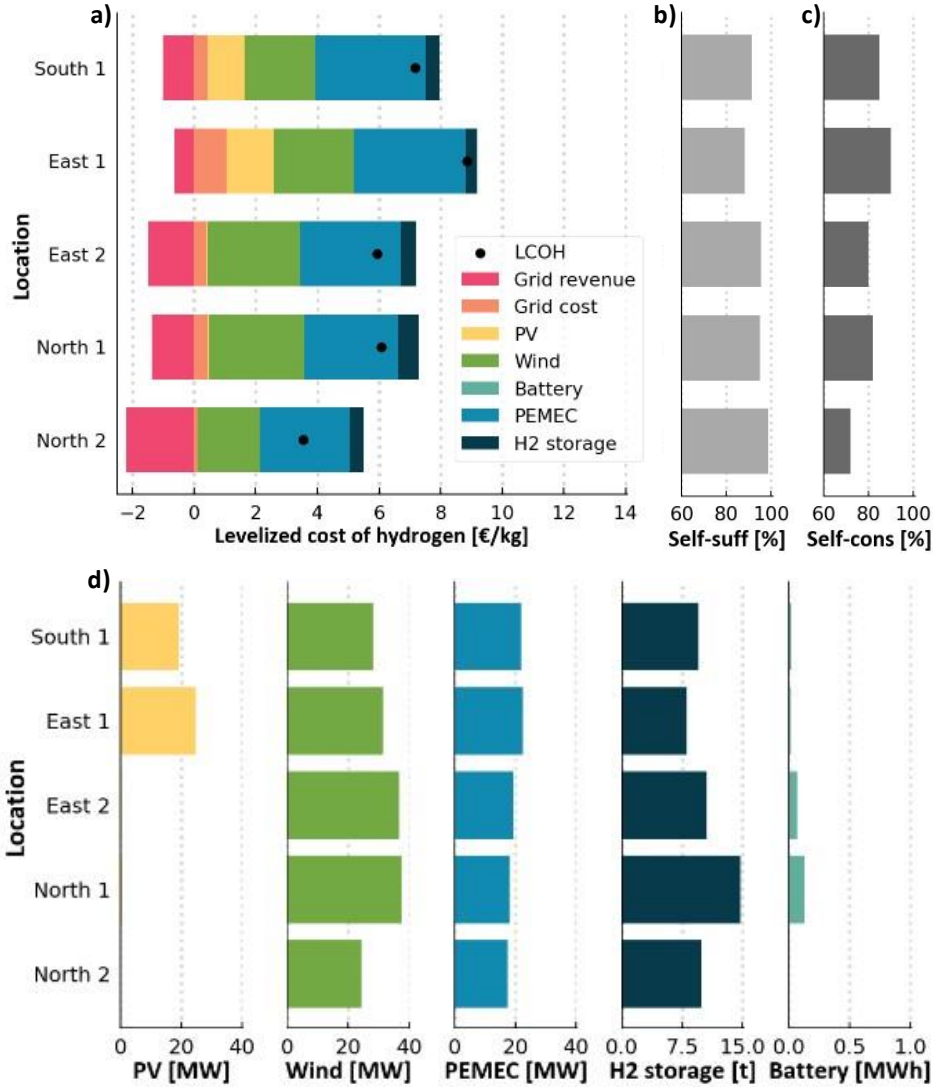

Figure 4: LCOH and optimized component sizes for the different European sites, based on an electricity cost of 150 €/MWh. a) The sale of electricity to the grid is subtracted from the cost, and this results in the final LCOH indicated with the black points. b) self-sufficiency of renewable electricity used by the electrolyzer c) self-consumption of renewable electricity by the electrolyzer d) sizes of the different components

Figure 4a analyzes the composition of the LCOH for the five representative European sites and depicts the corresponding results of the size optimization. The different cost contributions are indicated in a stacked form, while the revenues from electricity sales are subtracted. The final LCOH ranges from 3.5 €/kg to 8.9 €/kg. The lowest values are obtained for the North 2 location, which differentiates from the others, especially concerning electricity withdrawal, which, in this case, is very low. The LCOH composition at the East 1 and North 1 locations is very similar and reaches 6 €/kg. The South 1 and East 1 sites have the highest LCOH values, that is, of more than 7 €/kg.

The main cost contributions to LCOH for all the sites are the CAPEX of the electrolyzer and renewables. The electrolyzer size varies between 18 and 22 MW (Figure 4d), and this results in a cost of around 3 €/kg. The installed wind capacity is much more heterogeneous. Although only 24 MW is installed in the wind-rich climate of North 2, locations at higher latitudes, such as North 1 and East 2, require more than 36 MW of wind power, and this leads to a cost of 3 €/kg. The South 1 and East 1 locations, which are at a lower latitude, show more than 1300 PV full-load hours and incorporate solar PV capacities of 19 and 25 MW, respectively. This adds to the approximately 30 MW of wind turbines necessary for these locations and represents an additional cost factor.

Hydrogen storage accounts for a minor portion of the overall cost, and ranges between 0.4 and 0.7 €/kg. The largest storage capacity of 15 t is shown for North 1, while other sites range from 8 to 10.5 t. Battery installation has only a negligeable size in all of the scenarios. The highest battery capacity installed in all the sites, with 22 kW and 122 kWh, is witnessed for the North 1 site. However, this size is negligeable compared to the 38 MW of the wind turbines and can most likely be attributed to the metaheuristic nature of the algorithm. The driving force of the algorithm to not install battery storage is purely economic. The high capital cost of the components cannot be fully offset by its contribution to renewable electricity utilization.

Electricity withdrawal typically contributes by less than 0.5 €/kg to the total cost, and again has a lower impact in the wind rich northern European climates, where less reliance on the grid is necessary. The exception is location East 1, which experiences few full-load hours. This necessitates an increased withdrawal from the grid and leads to costs of 1 €/kg. Selling excess electricity significantly reduces the LCOH, despite this contribution not being included in the optimizer's objective function. The optimizer prioritizes installing more renewable energy to cover periods of lower production and minimizes grid withdrawal, and thus accepts leaving some of the self-produced electricity unutilized in other periods.

The effect of electricity withdrawal can also be seen in the plant's self-sufficiency (Figure 4b). At the North 2 site, nearly all hydrogen production can be covered by self-produced renewable electricity, whereas this ratio drops to 90 % at East 1. Additionally, self-consumption, or the share of the renewable electricity production used by the plant (Figure 4c), is much higher at East 1 compared to North 2. This indicates that locations with high renewable potential have better self-

sufficiency but also experience higher renewable overproduction, resulting in increased grid injections.

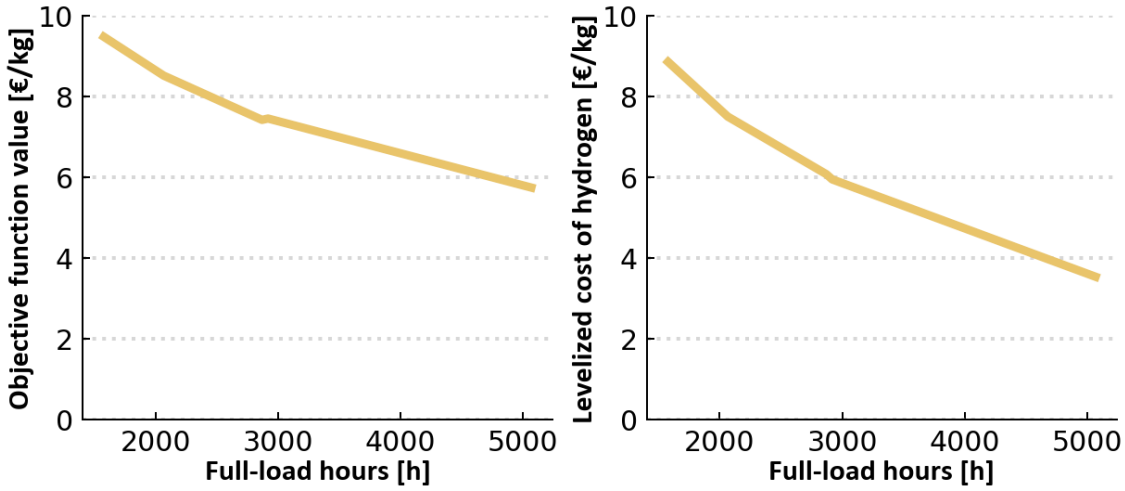

Figure 5: Objective function value (no electricity sale) and LCOH (including electricity sale) in function of the full-load hours

Figure 5 offers an overview of the achieved LCOH and the objective function (OBJ) values of the investigated locations. A clear trend of lower OBJ and LCOH for higher full-load hours is evident. Location East 1, which has the fewest full-load hours, has the highest OBJ, that is, of 9.4 €/kg. Electricity sale only slightly reduces the cost, as seen previously in Figure 4. Location South 1 achieves 2100 full-load hours, which results in an LCOH of 7.5 €/kg. East 2 and North 1, both of which are characterized by approximately 2900 full-load hours, reach an OBJ of 7.4 €/kg and an LCOH of 6 €/kg. Finally, the windy North 2 site achieves an OBJ of approximately 5 €/kg, with the sale of grid electricity further reducing the LCOH to 3.5 €/kg. A close correlation between the full-load hours and both OBJ and LCOH is generally observed.

3.2 Electricity cost sensitivity

The cost of grid electricity significantly impacts the sizing of a PtH system and has fluctuated a great deal in recent years. This chapter explores the sensitivity of key parameters, including system sizing, LCOH, and environmental indicators to variations in the cost of electricity.

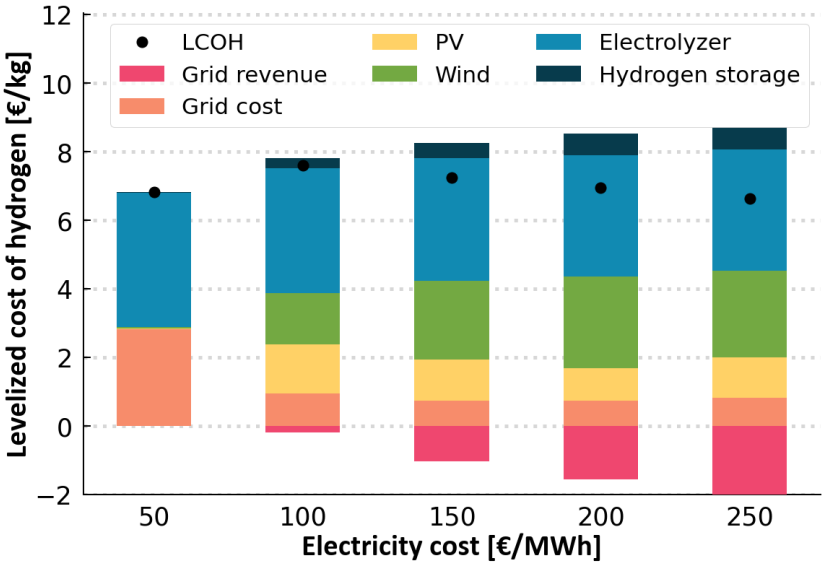

Figure 6: the composition of LCOH for different electricity prices for the South 1 renewable profile

Figure 6 offers a detailed breakdown of the composition of the LCOH for location South 1, which represents a typical southern European climate. This location incorporates both wind and solar PV, and therefore provides insights into the selection process for renewable energy sources.

The system is based entirely on grid electricity for a grid electricity price of 50 €/MWh. Renewables, which first consist of 18 MW wind turbines and 23 MWp solar PV, start to be installed from 100 €/MWh. As the electricity price further increases, the installation of wind turbines rises to over 30 MW, while solar PV power only decreases minimally. As the electricity price further increases, wind turbine installations rise to over 30 MW, while solar PV power decreases slightly. The nominal power of the electrolyzer reduces marginally from 23 MW, for the lowest electricity cost, to 21 MW for 250 €/MWh. The growth in hydrogen storage size can be observed together with the renewable installations, starting from 6 tons for 100 €/MWh and increasing to 14 tons for the highest investigated electricity cost. Consistent with the previous findings, the optimizer excludes battery storage from all the scenarios, as it would increase the LCOH.

The LCOH stands at 7.1 €/kg for a grid electricity price of 50 €/MWh. However, it further declines for electricity costs that exceed 100 €/MWh and reaches its minimum value of 6.8 €/kg for 250 €/MWh. The sale of electricity exerts a mitigating effect on the LCOH, particularly for higher electricity costs. Up to 100 €/MWh self-produced renewable energy is consumed almost entirely by the electrolyzer. This changes for higher electricity costs, as the renewable capacity increases. For instance, the sale of electricity reduces the LCOH by 2 €/kg for an electricity cost of 250 €/MWh. A negative correlation between the grid electricity costs and the expenses for renewable and hydrogen storage installations is generally observed. Installing a larger renewable capacity leads to a reduction in the withdrawal of electricity and is therefore preferred for higher electricity costs.

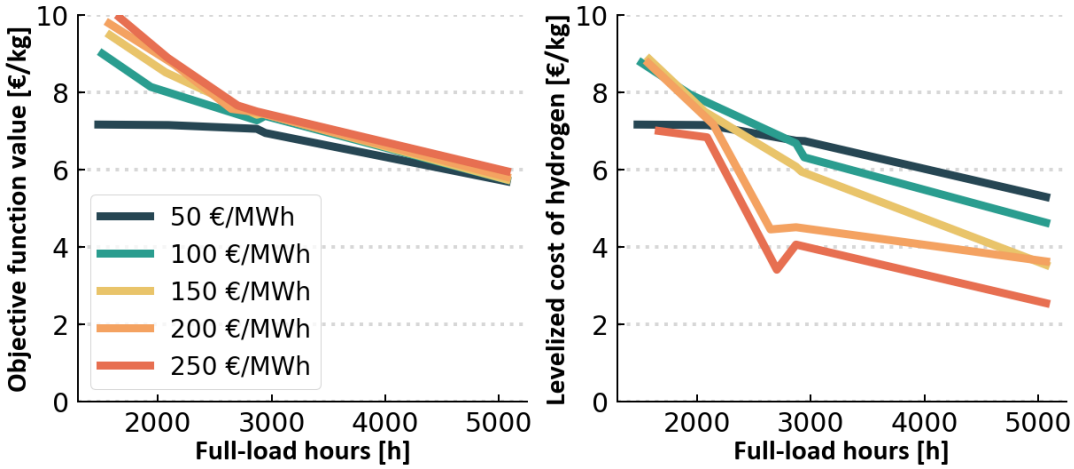

Figure 7: Objective function value (no sale of electricity) and LCOH (including the sale of electricity) for different full-load hours and electricity costs

Figure 7 offers an overview of the achieved LCOH and the objective function (OBJ) values for the five investigated locations. The OBJ shows a dependency on the full-load hours. Locations with fewer full-load hours, such East 1, have higher OBJ values, ranging between 7.2 and 10 €/MWh. The higher cost is mainly caused by the increase in the CAPEX to abate the cost of grid electricity. The windy North European site (North 2) achieves an OBJ of around 5.5 €/kg, regardless of the electricity prices. There are no notable differences at this site, as the system bases its electricity consumption on self-produced renewables, even for the 50 €/MWh scenario, due to the very low LCOE. Consequently, only a minimal amount of grid electricity is needed, and this leads to a minimal impact of variations of the grid prices.

Introducing the sale of electricity significantly reduces the LCOH, particularly for higher electricity prices. This effect is more pronounced in locations with abundant wind resources, such as East 2, North 1, and North 2. In these scenarios, the excess renewable electricity production significantly outweighs the electricity withdrawn from the grid. The lower LCOE of self-produced electricity, compared to grid electricity, incentivizes the optimization algorithm to prioritize larger renewable installations. This tendency is even more pronounced for higher electricity prices (200 and 250 €/MWh). Consequently, these scenarios experience the largest discrepancies between the LCOH and the objective function, reaching up to 4 €/kg. Additionally, these locations achieve the lowest absolute LCOH values, with North 2 and East 2 reaching less than 4 €/kg. The non-linearities of the LCOH can be partly attributed to the nature of the objection function, which can lead to very different LCOH outcomes for very similar OBJ results. For example, the downward spike in the LCOH at 2700 h for Location East 2 can be attributed to an increase in the installed RES capacity. Here, the algorithm for higher electricity costs than 150 €/MWh adds 7 MW of solar PV, while the wind power remains constant. This significantly increases the sale of electricity and leads to a plummeting of the LCOH.

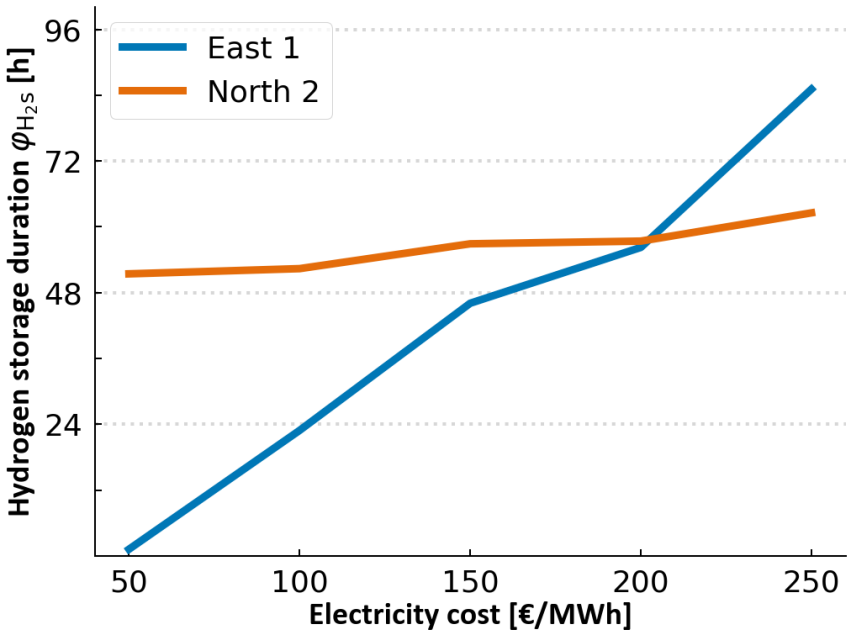

Figure 8: The duration of hydrogen storage for different electricity prices for the locations with the highest and lowest full-load hours

The duration of hydrogen storage, $\varphi_{H2st,}$ is depicted in Figure 8 and is calculated as the capacity of the hydrogen storage divided by the average hydrogen demand (Equation 11). The figure presents the results for the locations with the highest (North 2) and lowest (East 1) full-load hours. The storage durations of Locations North 1 and East 2 behave similarly to that of North 2, while South 1 follows a similar trend to that of East 1. The results for these locations can be found in Appendix A Figure A.3.

The storage duration tends to increase as the electricity prices rise. This occurs as the algorithm attempts to mitigate the need for withdrawal from the grid. The storage duration ranges from 0 to 84 h, with most cases exceeding one day. Although this duration exceeds the storage requirements of solar PV, which typically covers the nighttime demand, it is well aligned with the fluctuations in wind energy generation. No hydrogen storage is installed for the East 1 location for an electricity cost of 50 €/MWh. In this case, no renewable energy capacity is installed, thereby rendering hydrogen storage unnecessary. The storage duration across the locations differs by less than 30 % for higher electricity costs, while it diverges more for the low electricity cost scenarios.

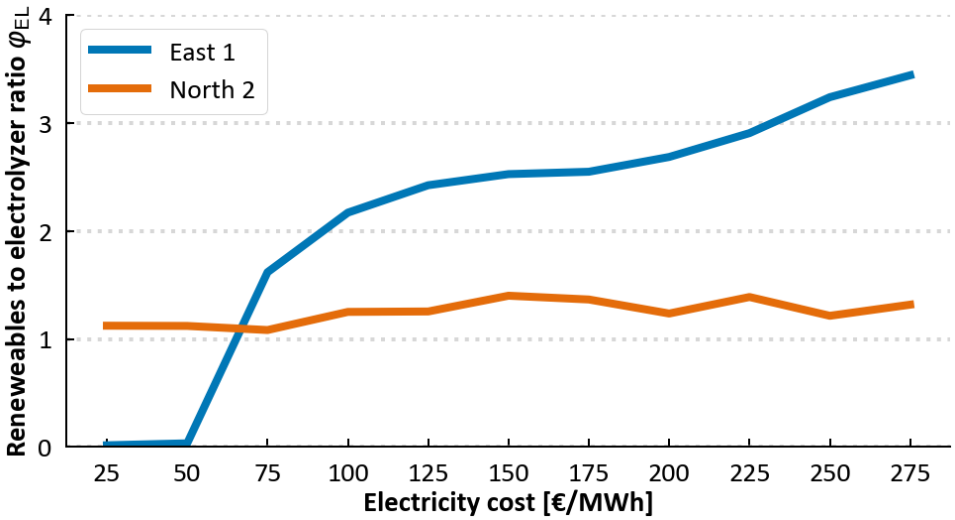

Figure 9:The renewables-to-electrolyzer ratio for different electricity prices for the locations with the highest and lowest full-load hours

Figure 9 presents the results of an analysis on the optimal ratio of the installed renewable capacity-to-the electrolyzer nominal power, φ_{EL}, for different electricity price scenarios. The graph shows the results for the extreme scenarios, which are representative of the locations with a low (East 1) and high (North 2) renewable potential.

The data reveals a pronounced trend of increasing installed renewable capacity at location East 1 for rising electricity prices. No renewable power is installed at East 1 for electricity prices of up to 50 €/MWh, where the optimal electrolyzer size is 23 MW. In this case, the algorithm prefers to rely on hydrogen production for low-cost grid electricity. The ratio of the renewables-to-the electrolyzer capacity (φ_{EL}) increases to more than 1.6 from 75 €/MWh onwards. This signifies that the renewable capacity becomes 1.6 times greater than the electrolyzer capacity. Instead, φ_{EL} reaches values of 2.5 at 150 €/MWh and 3.4 for the highest electricity price. This increase can primarily be attributed to a significant increase in the renewable installations of up to 70 MW, while the electrolyzer size remains stable. Furthermore, the renewable installations at location East 1 incorporate a substantial share of solar energy together with wind power, which tends to further increase the renewables-to-electrolyzer ratio. The rationale behind this result lies in the attempt of the algorithm to avoid expensive grid withdrawal through large-scale renewable energy production. This is accompanied by a large hydrogen storage capacity. This strategy enables the system to primarily rely on renewable electricity, without requiring an upsized electrolyzer. Since the electrolyzer constitutes a substantial portion of the total cost, this approach minimizes the overall expenditure of the system.

A contrasting trend emerges for location North 2, compared to the previous observation. Here, only a marginal increase in φ_{EL} is observed. The system is based to a great extent on renewable electricity, even for low electricity prices, and this results in $\varphi_{EL} > 1$. The wind turbine capacity increases by 15-20 % for electricity costs that exceed 100 €/MWh, reaching up to 24 MW. This represents a relatively minor capacity change, compared to the other locations. The electrolyzer size does not change significantly across the scenarios. Notably, the optimal system configuration

relies on the high number of full-load hours all year-round, making it unnecessary to over-install the renewable capacity to cover long periods with lower production.

A similar trend to that of East 1 can be observed for the remaining 3 locations, that is, South 1, East 2 and North 1. These locations share a comparable number of full-load hours. No renewable capacity is installed for 25 €/MWh, while these capacities increase for higher electricity prices and reach φ_{EL} values of 1.5 to 2.5. Detailed results of these remaining locations are presented in Appendix A Figure A.4.

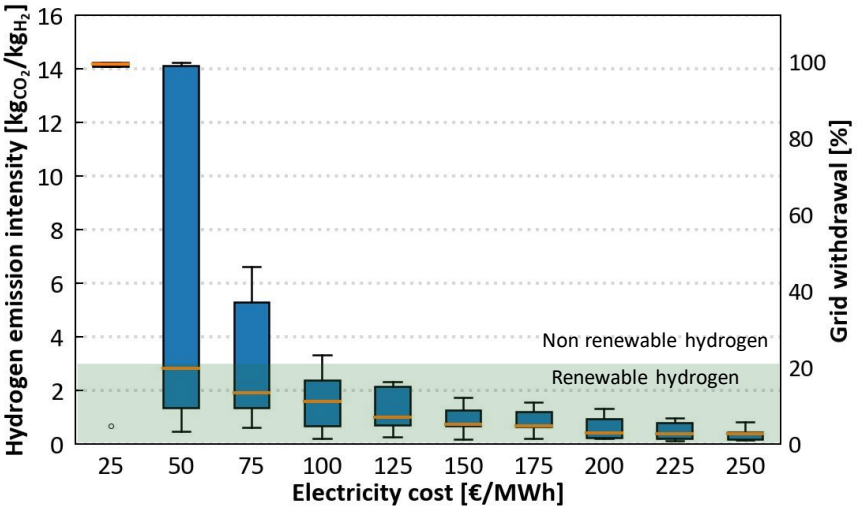

Figure 10: The hydrogen emission intensity for different electricity prices across the investigated locations

In order to be defined as RFNBO, according to EU definition, green hydrogen must satisfy the GHG saving threshold and lead to emissions of less than 3 kg_{CO2eq}/kg_{H2}. Figure 10 shows the emission intensity of the produced hydrogen, considering the average European grid emissions. Each box represents the emission intensity across the five sites for a specific electricity price, which is based on the cost of the optimal plant configurations.

The emission intensity of hydrogen depends to a great extent on the cost of electricity. Lower electricity prices incentivize the installation of fewer wind turbines or solar PV systems, and consequently increase the dependence on grid electricity. The emission intensity varies between 14.2 $kg_{CO2}/kg_{H2,}$ for the case of an electricity price of 25 €/MWh, and 0.1 kg_{CO2}/kg_{H2} for windy north European climates, to an electricity price that exceeds 200 €/MWh.

The most significant changes in emissions occur for electricity costs close to the levelized cost of electricity. LCOE values are obtained in the 24-70 €/MWh range, with the highest values being observed for location East 1 and the lowest for North 2. Less grid electricity is required for the same price point, due to the lower LCOE in renewable-rich locations, and this leads to a lower hydrogen emission intensity. This, in turn, results in a wide spread of the emission intensity across locations for an electricity cost of 50 or 75 €/MWh. Although most of the considered locations meet the hydrogen emission threshold for 50 €/MWh, South 1 requires an electricity price above 100 €/MWh, and East 1 necessitates a price of 125 €/MWh.

The emission intensities observed for all the locations for the scenarios with an electricity cost of at least 125 €/MWh comply with the GHG-saving threshold defined in Delegated Regulation (EU) 2023/1185. According to this regulation, no more than 20 % of the electricity used during electrolysis can originate from the electric grid to satisfy this threshold.

3.3 Variability in the hydrogen demand profiles

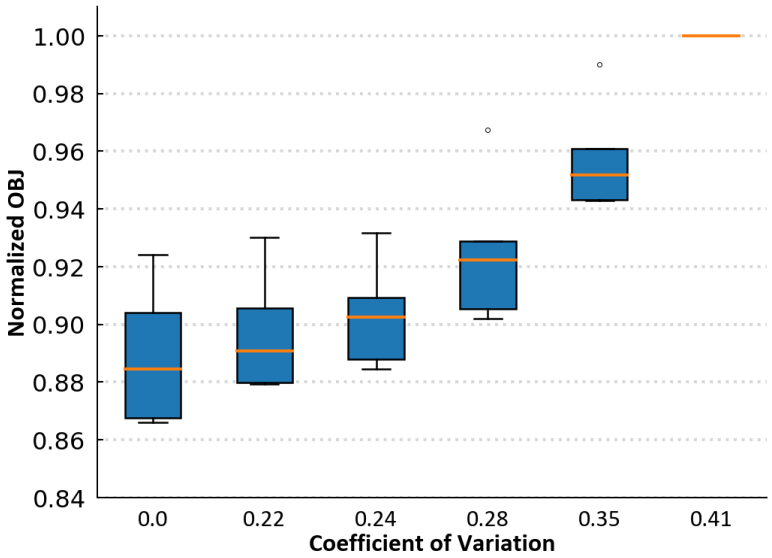

Figure 11: Normalized objective function values (OBJ, without the sale of electricity) for different day-to-day demand variabilities for an electricity cost of 150 €/MWh

Figure 11 shows the influence of fluctuations in the demand profile on the OBJ. Each box in the figure represents the results of a distinct hydrogen demand profile. The reader can refer to Chapter 2.2 for information on the generation of these profiles. Each box displays the normalized value of the OBJ for all of the considered sites with the corresponding demand profile. Normalization is performed with respect to the synthetical load profile of the base case, which has a coefficient of variation (CV) of 0.41.

The results show that a more constant demand profile reduces the cost across all the locations. There is an average reduction of 11 % in OBJ when transitioning from a profile with the initial condition (CV of 0.41) to a constant profile (CV of 0). The electrolyzer size on average reduces by 22 %, with respect to the baseline profile, when a constant demand profile is used. Most of this reduction already occurs for the profile with a CV of 0.22. The additional reduction induced by resorting to a constant profile is somewhat limited, compared to the importance of slightly decreasing the fluctuations in a highly variable profile. Significant PV installations are only present in the South 1 and East 3 locations, where a constant demand profile causes size reductions of 13 and 17 %, respectively. The wind turbine capacity is less sensitive to the profile variability of the demand and no clear trend has been observed. The hydrogen storage size is highly sensitive to the fluctuations of the demand profile. A less fluctuating demand reduces the possibility of leaving the demand unsatisfied, and a smaller hydrogen storage can manage the task. The storage capacity is

on average reduced by 50 % for the constant profile, compared to the baseline profile. However, as the contribution of the hydrogen storage to the total cost is limited, the electrolyzer size reduction is still the most important driving force. The reader can refer to Appendix A Figure A.5 for detailed information on the optimized sizes for the constant demand profile.

4. Discussion

In order to better assess the results, they are here discussed in more detail in a context with other findings from the literature and analyzed regarding the limitations and potential improvements. Although both wind and solar energy have been employed in this study, wind is clearly preferred by the algorithm, and it leads to lower costs. Solar PV is mainly installed at sites at lower latitudes, and which exceed 1300 PV full-load hours. The optimal solution for the other representative European locations relies entirely on wind energy. This finding is aligned with other findings, such as those of Hofrichter [23]. It is important to note that the capital cost of the solar PV of 1048 €/kWp used in this study is on the conservative side, compared to the values used in other research [21], [27]. Indeed, cost reductions of solar PV might lead to shifts in the PV-to-wind power ratio and strengthen the importance of solar electricity.

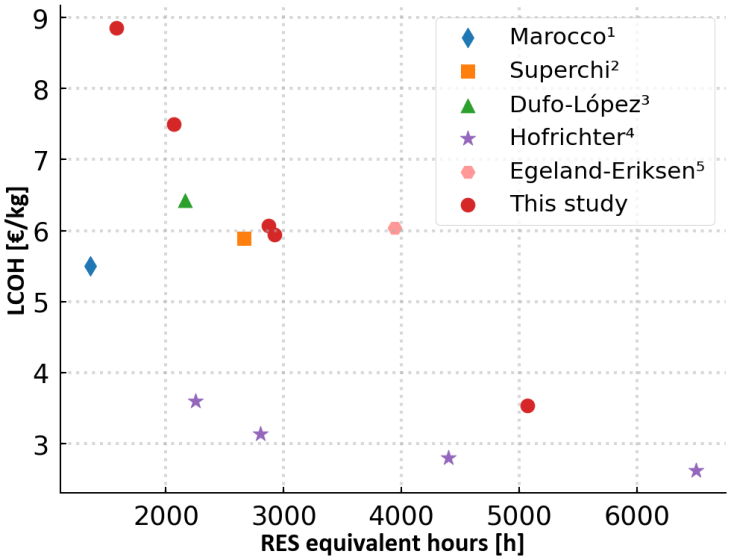

Figure 12: LCOH results of different PtH studies. The differences can be explained by considering the divergences in the starting assumptions. The assumptions differentiate, for example, in 1) 40 % lower CAPEX for the PV modules[27] 2) 40% lower electrolyzer cost [11] 3) taking into a consideration hourly variations of the electricity cost [21] 4) assuming an LCOE of 40 €/MWh across all the locations, independently of the full-load hours [23] 5) a case study that did not include size optimization [22]

Figure 12 presents an overview of the final LCOH results from various PtH studies. The LCOH in the baseline scenario ranges from 3.5 to 8.9 €/kg. The highest LCOH are observed for sites with a lower renewable potential, while high full-load hours significantly reduce the cost. The existing literature generally reports LCOH values in the range of 3-6 €/kg for comparable cost-optimal solutions [11], [21], [22], [23], [27]. Our results are roughly aligned with the literature, although they are slightly higher. These differences can be attributed to different input assumptions regarding the component costs, demand profiles, or other input hypothesis. The main differences are presented in the footnotes of the figure. Future works, in which more sites with different combinations of full-load hours should be analyzed, could further refine this evaluation. Additionally, if the sensitivities regarding the CAPEX of the components were to be considered, further insights would be obtained.

The optimal hydrogen storage capacity exceeds the intraday durations, thereby highlighting its advantage in providing multi-day flexibility at a low capital cost. If this result is compared with the optimal cost scenario of Superchi, it can be seen that this capacity duration is about twice as high [11]. Sensitivity studies with a flat demand profile indicate that these differences can likely be attributed to the higher fluctuations in the demand profile. Battery storage has not been found to bring an economic advantage. This result is in contrast with what was found in the studies of [16] in the context of microgrids. However, battery storage has a significant efficiency advantage in microgrids and can directly satisfy the electric load. This situation is hard to compare with a PtH system, where the users' demand is satisfied with hydrogen, and using batteries cannot avoid the energy conversion losses to hydrogen. The result, in agreement with other studies on PtH systems, is clearly in line with battery storage increasing the cost [19], [27]. However, the economics of battery storage could be more favorable in a non-grid connected system [20] or when a degradation function, which also considers the effect of load fluctuations, is included in the electrolyzer.

Our study demonstrates that the greenhouse gas emissions from the PtH system are likely to meet the EU threshold in most of the considered scenarios. The emissions in this study are slightly lower than those of Marocco and Superchi [11], [27], perhaps because of the higher number of full-load hours of the renewables. Moreover, the grid emission factor also plays a significant role. The average European electricity emission factor of 250 g/kWh has been used in this study, and this represents a simplification. Considering the EU's future electricity emission scenarios[40], a PtH system primarily powered by renewables and with grid electricity compensating for low renewable periods, will likely achieve the required greenhouse gas savings. However, significant variations exist between EU countries, making this aspect more challenging in some member countries that rely on fossil-based electricity production. In order to estimate a specific country's hydrogen emission intensity, our results can be multiplied by the ratio of the national electricity emission factor-to-the European emission factor. This approach is valid for regions with a similar renewable energy potential to those studied herein. However, a more comprehensive country-specific analysis would require evaluating a significantly larger number of locations. Moreover, an analysis based solely on emissions does not allow the produced hydrogen to be classified as renewable. Article 4 of Delegated Regulation (EU) 2023/1184 has established additional requirements, particularly regarding grid electricity, which must be met for such a classification [15]. Satisfying these conditions depends to a great extent on the specific bidding zone, but this is beyond the scope of the generalized approach of the present study.

To assess the reliability and accuracy of the results, we conducted multiple runs with the exact same inputs, leading to negligible differences in the LCOH. However, due to the complex nature of the objective function, very similar LCOH can be achieved with different combinations of component sizes on some occasions. Moreover, using an optimization-based control strategy could improve plant operation. In this study, all equipment investment costs are annualized, avoiding the computational expense of multiannual simulations. This approach is more conservative and may increase the LCOH as it assumes complete electrolyzer replacement after its lifetime instead of multiannual stack replacements. Nonetheless, when comparing the results to other studies,

assumptions on CAPEX and equipment selection have a significant impact, likely surpassing the aforementioned aspects.

5. Conclusions

This work provides the results of a techno-economic analysis of a power-to-hydrogen system used to supply high-temperature heat to a hard-to-abate industrial site. We have developed a methodology to size, optimize, and simulate the electrolyzer, PV, and wind energy capacity, along with hydrogen storage, over a one-year simulation with an hourly resolution. The industrial site, electrolyzer, and renewable production were modelled considering different representative locations across Europe, to facilitate the generalization of a variety of investigated features. The study has also applied a methodology to generate synthetic thermal load profiles and has investigated the effect of different degrees of demand variability. The main results are:

- Wind energy plays a dominant role in most of the considered European sites as the electricity source for PtH and allows the LCOH to be reduced, reaching a cost of between 3.4 €/kg in a windy north European climate and 8.9 €/kg in an eastern European location with fewer full-load hours. Solar PV only leads to a significant cost reduction in the south European climates, but hardly any benefit has been observed for the windy northern European sites, where it is outperformed by the higher full-load hours of wind turbines.
- Hydrogen storage is able to satisfy the average hydrogen demand for more than 24 hours, if the system is based on a significant share of renewables. For most cases, the storage durations are in the 50-to-80-hour range, which allows periods of lower wind availability to be covered. The storage duration increases for higher electricity costs, as this improves the utilization of renewable energy. Battery storage has been found to not be cost optimal in any of the scenarios.
- The hydrogen carbon emission intensity depends on the price of the grid electricity. Indeed, it is cost-effective to make most of the hydrogen production rely on self-produced renewable electricity for electricity costs above 100 €/MWh. In these scenarios, the hydrogen emission intensity limit of 3 kg_{CO2}/kg_{H2} is satisfied. It is more challenging to satisfy the emission requirement for lower grid electricity costs.
- Fluctuations in the hydrogen demand profile are associated with higher costs, as the demand peaks need to be covered by an oversizing of the plant components. Although small demand fluctuations play a minor role, a profile with a coefficient of variation of 0.41 increases the OBJ values by approximately 12 %, compared to a constant demand profile.

On the basis of the results of this study, future work should expand the geographical scope to other world regions and investigate more locations in order to facilitate generalization. Furthermore, including optimization in the control strategy could lead to a significant improvement of the system, as it would help increase the modelling precision.

Acknowledgements

We would like to thank Mateo Jesper for his assistance in generating the synthetic load profiles.

M. Stolte carried out this study as part of the PNRR-NGEU project, which has received funding from the MUR – DM 117/2023. The scholarship is co-funded by Edison S.p.A.

F.D. Minuto carried out this study within Ministerial Decree no. 1062/2021 and received funding from the FSE REACT-EU - PON Ricerca e Innovazione, 2014-2020.

A. Lanzini carried out this study within the National Recovery and Resilience Plan (PNRR) and received funding from the Italian Ministry of the Environment and Energy Security, the "Novel Materials for Hydrogen storage (NoMaH)" project, ID RSH2A_000035, CUP: F27G22000180006.

This manuscript only reflects the authors' views and opinions, and neither the European Union nor the European Commission can be considered responsible for them.

Bibliography

[1] ‘Tracking Clean Energy Progress - Industry’, International Energy Agency. Accessed: Feb. 14, 2024. [Online]. Available: https://www.iea.org/energy-system/industry

[2] ‘Assessment of green hydrogen for industrial heat’, Deloitte, 2023. Accessed: Nov. 13, 2023. [Online]. Available: https://www2.deloitte.com/us/en/pages/energy-and-resources/articles/green-hydrogen.html

[3] Y. Guo *et al.*, ‘A review of low-carbon technologies and projects for the global cement industry’, *J. Environ. Sci.*, vol. 136, pp. 682–697, Feb. 2024, doi: 10.1016/j.jes.2023.01.021.

[4] ‘Best available techniques reference document: Ceramic Manufacturing Industry’, European Commission, 2007. Accessed: Feb. 14, 2024. [Online]. Available: https://eippcb.jrc.ec.europa.eu/reference/ceramic-manufacturing-industry

[5] M. D. Obrist, R. Kannan, T. J. Schmidt, and T. Kober, ‘Long-term energy efficiency and decarbonization trajectories for the Swiss pulp and paper industry’, *Sustain. Energy Technol. Assess.*, vol. 52, p. 101937, Aug. 2022, doi: 10.1016/j.seta.2021.101937.

[6] M. A. Habib, G. A. Q. Abdulrahman, A. B. S. Alquaity, and N. A. A. Qasem, ‘Hydrogen combustion, production, and applications: A review’, *Alex. Eng. J.*, vol. 100, pp. 182–207, Aug. 2024, doi: 10.1016/j.aej.2024.05.030.

[7] A. Palacios and D. Bradley, ‘Conversion of natural gas jet flame burners to hydrogen’, *Int. J. Hydrog. Energy*, vol. 46, no. 33, pp. 17051–17059, May 2021, doi: 10.1016/j.ijhydene.2021.02.144.

[8] L. Giannuzzo, F. D. Minuto, D. S. Schiera, and A. Lanzini, ‘Reconstructing hourly residential electrical load profiles for Renewable Energy Communities using non-intrusive machine learning techniques’, *Energy AI*, vol. 15, p. 100329, Jan. 2024, doi: 10.1016/j.egyai.2023.100329.

[9] M. Jesper, F. Pag, K. Vajen, and U. Jordan, ‘Annual Industrial and Commercial Heat Load Profiles: Modeling Based on k-Means Clustering and Regression Analysis’, *Energy Convers. Manag. X*, vol. 10, p. 100085, Jun. 2021, doi: 10.1016/j.ecmx.2021.100085.

[10] M. Benghanem *et al.*, ‘Hydrogen Production Methods Based on Solar and Wind Energy: A Review’, *Energies*, vol. 16, no. 2, Art. no. 2, Jan. 2023, doi: 10.3390/en16020757.

[11] F. Superchi, A. Mati, C. Carcasci, and A. Bianchini, ‘Techno-economic analysis of wind-powered green hydrogen production to facilitate the decarbonization of hard-to-abate sectors: A case study on steelmaking’, *Appl. Energy*, vol. 342, p. 121198, Jul. 2023, doi: 10.1016/j.apenergy.2023.121198.

[12] H. Shen, P. Crespo del Granado, R. S. Jorge, and K. Löffler, ‘Environmental and climate impacts of a large-scale deployment of green hydrogen in Europe’, *Energy Clim. Change*, vol. 5, p. 100133, Dec. 2024, doi: 10.1016/j.egycc.2024.100133.

[13] E. A. Nanaki, S. Kiartzis, and G. Xydis, ‘Is Greece Ready for a Hydrogen Energy Transition?—Quantifying Relative Costs in Hard to Abate Industries’, *Energies*, vol. 17, no. 7, Art. no. 7, Jan. 2024, doi: 10.3390/en17071722.

[14] J. Brandt *et al.*, ‘Cost and competitiveness of green hydrogen and the effects of the European Union regulatory framework’, *Nat. Energy*, pp. 1–11, May 2024, doi: 10.1038/s41560-024-01511-z.

[15] EU, *COMMISSION DELEGATED REGULATION (EU) 2023/1184*. 2023. Accessed: Sep. 05, 2023. [Online]. Available: https://eur-lex.europa.eu/legal-

content/EN/TXT/?toc=OJ%3AL%3A2023%3A157%3ATOC&uri=uriserv%3AOJ.L_.2023.157.01.0011.01.ENG

[16] S. Hajiaghasi, A. Salemnia, and M. Hamzeh, 'Hybrid energy storage system for microgrids applications: A review', *J. Energy Storage*, vol. 21, pp. 543–570, Feb. 2019, doi: 10.1016/j.est.2018.12.017.

[17] E. Rozzi, F. D. Minuto, and A. Lanzini, 'Dynamic modeling and thermal management of a Power-to-Power system with hydrogen storage in microporous adsorbent materials', *J. Energy Storage*, vol. 41, p. 102953, Sep. 2021, doi: 10.1016/j.est.2021.102953.

[18] R. Novo, F. D. Minuto, G. Bracco, G. Mattiazzo, R. Borchiellini, and A. Lanzini, 'Supporting Decarbonization Strategies of Local Energy Systems by De-Risking Investments in Renewables: A Case Study on Pantelleria Island', *Energies*, vol. 15, no. 3, Art. no. 3, Jan. 2022, doi: 10.3390/en15031103.

[19] V. A. Martinez Lopez, H. Ziar, J. W. Haverkort, M. Zeman, and O. Isabella, 'Dynamic operation of water electrolyzers: A review for applications in photovoltaic systems integration', *Renew. Sustain. Energy Rev.*, vol. 182, p. 113407, Aug. 2023, doi: 10.1016/j.rser.2023.113407.

[20] A. Ibanez-Rioja and P. Kauranen, 'Off-grid solar PV–wind power–battery–water electrolyzer plant: Simultaneous optimization of component capacities and system control', *Appl. Energy*, vol. 345, p. 121277, Sep. 2023, doi: 10.1016/j.apenergy.2023.121277.

[21] R. Dufo-López, J. M. Lujano-Rojas, and J. L. Bernal-Agustín, 'Optimisation of size and control strategy in utility-scale green hydrogen production systems', *Int. J. Hydrog. Energy*, Sep. 2023, doi: 10.1016/j.ijhydene.2023.08.273.

[22] T. Egeland-Eriksen and S. Sartori, 'Techno-economic analysis of the effect of a novel price-based control system on the hydrogen production for an offshore 1.5 GW wind-hydrogen system', *Energy Rep.*, vol. 11, pp. 2633–2655, Jun. 2024, doi: 10.1016/j.egyr.2024.02.016.

[23] A. Hofrichter, D. Rank, M. Heberl, and M. Sterner, 'Determination of the optimal power ratio between electrolysis and renewable energy to investigate the effects on the hydrogen production costs', *Int. J. Hydrog. Energy*, vol. 48, no. 5, pp. 1651–1663, Jan. 2023, doi: 10.1016/j.ijhydene.2022.09.263.

[24] H. Elsheikh and V. Eveloy, 'Assessment of variable solar- and grid electricity-driven power-to-hydrogen integration with direct iron ore reduction for low-carbon steel making', *Fuel*, vol. 324, p. 124758, Sep. 2022, doi: 10.1016/j.fuel.2022.124758.

[25] H. Elsheikh and V. Eveloy, 'Renewable hydrogen based direct iron ore reduction and steel making with grid assistance', *Energy Convers. Manag.*, vol. 297, p. 117544, Dec. 2023, doi: 10.1016/j.enconman.2023.117544.

[26] P. Marocco, M. Gandiglio, D. Audisio, and M. Santarelli, 'Assessment of the role of hydrogen to produce high-temperature heat in the steel industry', *J. Clean. Prod.*, vol. 388, p. 135969, Feb. 2023, doi: 10.1016/j.jclepro.2023.135969.

[27] P. Marocco, M. Gandiglio, and M. Santarelli, 'Optimal design of PV-based grid-connected hydrogen production systems', *J. Clean. Prod.*, vol. 434, p. 140007, Jan. 2024, doi: 10.1016/j.jclepro.2023.140007.

[28] S. Mingolla *et al.*, 'Effects of emissions caps on the costs and feasibility of low-carbon hydrogen in the European ammonia industry', *Nat. Commun.*, vol. 15, no. 1, p. 3753, May 2024, doi: 10.1038/s41467-024-48145-z.

[29] L. Miranda, 'Pyswarms Library'. Apr. 17, 2024. Accessed: Apr. 17, 2024. [Online]. Available: https://github.com/ljvmiranda921/pyswarms

[30] J. Bergstra and Y. Bengio, ‘Random Search for Hyper-Parameter Optimization’, 2012.
[31] Solargis, ‘Global Solar Atlas 2.0’. 2024. [Online]. Available: https://globalsolaratlas.info
[32] N. N. Davis *et al.*, ‘The Global Wind Atlas: A High-Resolution Dataset of Climatologies and Associated Web-Based Application’, *Bull. Am. Meteorol. Soc.*, vol. 104, no. 8, pp. E1507–E1525, Aug. 2023, doi: 10.1175/BAMS-D-21-0075.1.
[33] ‘Standard country or area codes for statistical use (M49)’. 1999. Accessed: Apr. 17, 2024. [Online]. Available: https://unstats.un.org/unsd/methodology/m49/
[34] I. Staffell, ‘API - Renewables.ninja’. Accessed: Jan. 25, 2024. [Online]. Available: https://www.renewables.ninja/documentation/api
[35] ‘JRC Photovoltaic Geographical Information System (PVGIS) - European Commission’. Accessed: Jan. 25, 2024. [Online]. Available: https://re.jrc.ec.europa.eu/pvg_tools/en/
[36] I. Staffell and S. Pfenninger, ‘Using bias-corrected reanalysis to simulate current and future wind power output’, *Energy*, vol. 114, pp. 1224–1239, Nov. 2016, doi: 10.1016/j.energy.2016.08.068.
[37] Eurostat, ‘Electricity prices for non-household consumers - bi-annual data (from 2007 onwards)’. Accessed: Jan. 23, 2024. [Online]. Available: https://ec.europa.eu/eurostat/databrowser/view/nrg_pc_205/default/table?lang=en
[38] Bundesnetzagentur, ‘SMARD | Wholesale prices’. Accessed: Feb. 20, 2024. [Online]. Available: https://www.smard.de/page/en/wiki-article/5884/5976
[39] *Commission Delegated Regulation (EU) 2023/1185 of 10 February 2023*. 2023. Accessed: Nov. 09, 2023. [Online]. Available: http://data.europa.eu/eli/reg_del/2023/1185/oj/eng
[40] European Environmental Energy Agency, ‘Greenhouse gas emission intensity of electricity generation in Europe’. Accessed: Feb. 20, 2024. [Online]. Available: https://www.eea.europa.eu/en/analysis/indicators/greenhouse-gas-emission-intensity-of-1
[41] M. Rezaei, A. Akimov, and E. MacA. Gray, ‘Economics of renewable hydrogen production using wind and solar energy: A case study for Queensland, Australia’, *J. Clean. Prod.*, vol. 435, p. 140476, Jan. 2024, doi: 10.1016/j.jclepro.2023.140476.
[42] M. Kopp, D. Coleman, C. Stiller, K. Scheffer, J. Aichinger, and B. Scheppat, ‘Energiepark Mainz: Technical and economic analysis of the worldwide largest Power-to-Gas plant with PEM electrolysis’, *Int. J. Hydrog. Energy*, vol. 42, no. 19, pp. 13311–13320, May 2017, doi: 10.1016/j.ijhydene.2016.12.145.
[43] A. J. Gee, D. B. Proud, N. Smith, A. Chinnici, and P. R. Medwell, ‘Hydrogen addition to a commercial self-aspirating burner and assessment of a practical burner modification strategy to improve performance’, *Int. J. Hydrog. Energy*, vol. 49, pp. 59–76, Jan. 2024, doi: 10.1016/j.ijhydene.2023.06.230.
[44] ‘Utility-scale batteries – Innovation Landscape Brief’, International Renewable Energy Agency, Abu Dhabi, 2019.
[45] National Renewable Energy Laboratory, ‘Electricity Annual Technology Baseline (ATB) Data 2022’, National Renewable Energy Laboratory, 2022. Accessed: Jan. 23, 2024. [Online]. Available: https://atb.nrel.gov/electricity/2022/data
[46] C. Lauterbach, *Potential, system analysis and preliminary design of low-temperature solar process heat systems*. kassel university press, 2014. doi: 10.17170/kobra-202308228664.
[47] ‘BAT reference documents | Eippcb’. Accessed: Apr. 17, 2024. [Online]. Available: https://eippcb.jrc.ec.europa.eu/reference
[48] F. A. Plazas-Niño, R. Yeganyan, C. Cannone, M. Howells, B. Borba, and J. Quirós-Tortós, ‘Assessing the role of low-emission hydrogen: A techno-economic database for hydrogen

pathways modelling', *Data Brief*, vol. 52, p. 109822, Feb. 2024, doi: 10.1016/j.dib.2023.109822.
[49] H. Grimm, Gunter Marius, 'Cost Forecast for Low-Temperature Electrolysis - Technology Driven Bottom-Up Prognosis for PEM and Alkaline Water Electrolysis Systems', Fraunhofer Institute for Solar Energy Systems ISE, 2021.
[50] R. R. Urs, A. Chadly, A. Al Sumaiti, and A. Mayyas, 'Techno-economic analysis of green hydrogen as an energy-storage medium for commercial buildings', *Clean Energy*, vol. 7, no. 1, pp. 84–98, Feb. 2023, doi: 10.1093/ce/zkac083.
[51] 'Gestore Mercati Energetici Electricity Market statistics'. Accessed: Sep. 06, 2023. [Online]. Available: https://www.mercatoelettrico.org/En/download/DatiStorici.aspx